2012-05

Optically pump-induced athermal and nonresonant refractive index changes in the reference Cr-doped laser materials: Cr:GSGG and ruby

Journal of the Optical Society of America B,Washington, DC : Optical Society of America - OSA,v. 29, n. 5, p. 1055-1064, May 2012
http://www.producao.usp.br/handle/BDPI/49923

Optically pump-induced athermal and nonresonant refractive index changes in the reference Cr-doped laser materials: Cr:GSGG and ruby

Thomas Godin,[1] Richard Moncorgé,[1] Jean-Louis Doualan,[1] Mickael Fromager,[1] Kamel Ait-Ameur,[1] Renato Antonio Cruz,[2] and Tomaz Catunda[2,*]

[1]*Centre de Recherche sur les Ions, les Matériaux et la Photonique (CIMAP), UMR 6252 CEA-CNRS-ENSICAEN, Université de Caen, France*
[2]*Institute of Physics of São Carlos, USP—São Carlos, São Paulo 13560-970, Brazil*
**Corresponding author: tomaz@ifsc.usp.br*

Received October 6, 2011; revised December 20, 2011; accepted December 28, 2011; posted January 3, 2012 (Doc. ID 156017); published April 23, 2012

The refractive index of most ion-doped materials increases with the excited state population. This effect was studied in many laser materials, particularly those doped with Cr^{3+} and rare earth ions, using several techniques, such as interferometry, wave mixing, and Z-scans. This refractive index variation is athermal (has an electronic origin) and is associated with the difference in the polarizabilites of the Cr^{3+} ion in its excited and ground states, $\Delta\alpha_p$. The Cr^{3+} optical transitions in the visible domain are electric-dipole forbidden, and they have low oscillator strengths. Therefore, the major contribution to $\Delta\alpha_p$ has been assigned to allowed transitions to charge transfer bands (CTBs) in the UV with strengths ~3 orders of magnitude higher. Although this CTB model qualitatively explains the main observations, it was never quantitatively tested. In order to further investigate the physical origin of $\Delta\alpha_p$ in Cr^{3+}-doped crystals, excited state absorption (ESA) and Z-scan measurements were thus performed in $Cr:Al_2O_3$ (ruby) and Cr:GSGG. Cr:GSGG was selected because of the proximity of its ^2E and $^4T_2$ emitting levels, and thus the possibility to explore the role of the spin selection rule in the ESA spectra and the resulting variations in polarizability by comparing low and room temperature data, which were never reported before. On the other hand, $Cr:Al_2O_3$ (ruby) was selected because it is the only crystal for which it is possible to obtain CTB absorption data from both ground and excited states, and thus for which it is possible to check the CTB model more accurately. Thanks to these more accurate and more complete data, we came to the first conclusion that the spin selection rule does not play any significant role in the variation of the polarizability with the ^2E–$^4T_2$ energy mismatch. We also discovered that using the CTB model in the case of ruby would lead to a negative $\Delta\alpha_p$ value, which is contrary to all refractive index variation (including Z-scan) measurements.

OCIS codes: 160.3380, 160.4760, 190.4720, 190.4223, 190.2055.

1. INTRODUCTION

Shortly after the operation of the first solid-state lasers, it became clear that refractive index changes, caused by high power operation of the active media, could have a tremendous impact on all main aspects of laser behavior. Optical distortions, for instance, virtually preclude diffraction-limited laser operation, even if the materials themselves are of diffraction-limited optical quality [1,2]. It also became clear that there are different kinds of refractive index changes, thermal and athermal, which are thus of purely electronic origin, due to the host materials and the active ions [3]. The refractive index changes due to the thermal heating and the electronic nonlinearity of the host materials were extensively studied and became a classical subject of laser engineering of solid-state lasers [1]. However, the contribution of the active ions to the electronic refractive index changes are not so well understood—not only their effects on laser operation [4] but also their physical or spectroscopic origin, which is the main subject of this paper.

In fact, the first laser-induced grating (LIG) experiment that can be related to some refractive index change was performed in 1967 in order to experimentally demonstrate the effect of spatial hole-burning in a ruby laser cavity [2]. In another experiment a frequency shift in a ruby laser was observed, which increased with the laser peak power [5]. It was shown that this shift appeared due to a refractive index variation that was proportional to the variation of the excited state population. Pohl [6] then explained this effect by a polarizability difference ($\Delta\alpha_p$) between the excited and ground states of ruby coming from the interaction with a charge transfer band (CTB). Ruby, indeed, has several weak absorptions bands in the visible with low oscillator strengths ($f \sim 10^{-4}$–10^{-5}), but also a very strong ($f \geq 0.1$) electric-dipole-allowed one peaking around ~57.000 cm^{-1} (6.9 eV or 175 nm). This band is attributed to a ligand (O^{2-})-to-metal (Cr^{3+}) charge transfer transition and would give the major contribution to $\Delta\alpha_p$.

Since then, ruby has been used as a test material for many experiments in nonlinear optics such as transient gratings, bistability, phase conjugation, two-wave mixing, Z-scans, and also slow light (see [7] and references therein). It is a convenient material because its ^2E metastable excited state can be pumped easily in the continuous-wave (CW) regime due to its long emission lifetime (~3.4 ms), either via its blue-green and broad $^4T_2$ and $^4T_1$ absorption bands or directly via its ^2E excited level.

Venkatesan and McCall [8] used ruby for the first demonstration of optical bistability at room temperature in a solid by directly pumping the R lines (~694 nm). Because of resonant pumping, they expected a cancellation of the two R line

contributions, which should have dispersive line shapes. However, this cancelation was not observed, so this behavior was attributed to a predominance of the nonresonant character of the nonlinearity, which was explained by the CTB contribution. This kind of nonresonant behavior was also noticed by Liao and Bloom [9] in their first report of phase conjugation by degenerate four-wave mixing. In their theoretical analysis, the authors concluded that the refractive index grating, also called the dispersive grating, instead of the absorption grating, gives the dominant contribution to the process. The first quantitative measurement of the nonlinearity in ruby was made using an interferometric technique [10] that conclusively demonstrated the dispersive origin of the phase conjugation, since it was measured that the real part of the refractive index change was 1 order of magnitude larger than the imaginary one. From this result, it was found that the polarizability difference between excited and ground states of ruby is $\Delta\alpha_p = 1.6 \times 10^{-25}$ cm^3, a value which was later confirmed by several experiments [4,7,11–15]. For instance, the dispersive character of ruby's nonlinearity was demonstrated with the nondegenerate two-wave mixing (NDTWM) experiments of McMichael *et al.* [11]. As opposed to degenerate wave mixing, NDTWM could discriminate the real and imaginary parts of the nonlinear refractive index n_2, through the parameter $r = n_2''/n_2'$. For ruby, it was found that $r \sim 0$ at 488 nm and $r \sim -0.1$ at 580 nm.

The question of the character (absorptive or refractive) and the sign of the nonlinearity is very important for practical applications, not only in nonlinear optics but also in lasers [16]. Therefore, some papers tried to investigate the Cr^{3+} nonlinearity from a spectroscopic point of view to further understand its physical origin. Weaver and Payne [17], for instance, determined the $\Delta\alpha_p$ value of Cr^{3+} in 10 different host crystals. They observed that $\Delta\alpha_p$ is 1 order of magnitude smaller in fluorides compared to oxides, and they attributed this behavior to the absence in the fluorides of any CTB transitions, at least in the near-UV spectral domain. Adler and Lawandy [12] performed NDTWM in ruby in order to test the CTB origin of the nonlinearity. They noticed that in the case of a resonance interaction, $n_2'(\nu)$ would have a dispersive line shape ($n_2' < 0$ for $\nu < \nu_o$ and $n_2' > 0$ for $\nu > \nu_o$) and approximately the same magnitude of n_2''. They investigated the wavelength dependence along the $^4T_2$ broadband (565–610 nm spectral range), and they found that $n_2'(\nu)$ is proportional to the absorption spectrum, thus indicating an approximately constant $\Delta\alpha_p(\nu)$ value within this spectral range. Moreover, no change in the spectrum of $\Delta\alpha_p$was observed when the crystal was cooled down to 77 K, although the linewidth of the ruby's R lines decreases by ~2 orders of magnitude. Since the CTB states do not change with temperature, this behavior also supported the nonresonant character and the CTB model for $\Delta\alpha_p$. The spectral dependence of $\Delta\alpha_p(\nu)$ in a wide spectral range, from 9000 to 21,000 cm^{-1}, was also determined using four-wave mixing in three Cr^{3+} doped crystals by Powell and Payne [18]. Their $\Delta\alpha_p(\nu)$ curves were then fitted with a single oscillator model, assuming that the lowest-energy CTB transition gave the dominant contribution to $\Delta\alpha_p(\nu)$. According to these authors, their result "provides the first direct and conclusive evidence for this (CTB) model." Finally, the $n_2(\lambda)$ spectroscopy was investigated across the R lines of ruby and alexandrite by using a variant of the Z-scan technique [7,14]. The results of [7], more particularly, allowed a clear discrimination of the resonant and nonresonant contributions to Δn. For ruby, it was observed that the nonresonant contribution to n_2 was 1 order of magnitude larger than the resonant one.

In this paper we intend to further address the physical origin of $\Delta\alpha_p$ in two important Cr^{3+}-doped crystals: Cr:GSGG and Cr:Al_2O_3 (ruby). Although ruby was already investigated in several experiments, several questions still persist: (i) as to the importance of the selection rules (between spin doublets and quartets) of the optical transitions that are invoked to account for $\Delta\alpha_p$ and (ii) as to the quantum-mechanical model that is generally used to relate $\Delta\alpha_p$ to the oscillator strengths of the involved UV transitions (according to the CTB model). The case of Cr:GSGG is particularly interesting because of the proximity of its ^2E and $^4T_2$ emitting levels, which makes the $^4T_2$ level thermally populated at room temperature, which is not the case for ruby. Therefore, the role of the selection rules can be addressed by investigating the temperature dependence of $\Delta\alpha_p$. Three types of experiments have been performed: (i) Z-scan measurements to determine $\Delta\alpha_p$ and its temperature dependence, especially in the case of Cr:GSGG, (ii) low and high temperature excited state absorption (ESA) measurements in the case of Cr:GSGG, and (iii) more reliable ESA measurements both in the visible and the near-UV spectral domains, especially in the case of ruby, in order to reach unquestionable values for the oscillator strengths of the considered ground state absorption (GSA) and ESA transitions. Although the past works have systematically assumed that the oscillator strengths of the UV transitions of Cr^{3+} in the ground and excited states of the ions were nearly equal, it is demonstrated here that these oscillator strengths can differ by 1 order of magnitude.

2. THEORETICAL GROUND

As mentioned in Section 1, athermal refractive index changes due to the active ion polarizability can be analyzed, considering the susceptibility as

$$\chi = \chi_m + N_g\alpha_{pg} + N_{ex}\alpha_{pex}, \tag{1}$$

where χ_m represents the host matrix's susceptibility, α_{pg} (α_{pex}) is the ground (excited) state polarizability, and N_g (N_{ex}) is the ground (excited) state population density. We are assuming that the medium has only one metastable excited level, whose lifetime is much longer compared to the other excited states. Therefore, in the CW regime only the ground state and the metastable excited state are significantly populated, so that $N_t \sim N_g + N_{ex}$. This is the case of ruby (Cr^{+3}:Al_2O_3) when it is optically pumped, for instance, by a green photon in resonance with the $^4T_2$ absorption band, and where the system rapidly relaxes (~picoseconds) to the ^2E metastable level.

We are interested in the refractive index change produced by the excited state population, so the local field effect should be introduced as

$$\frac{n^2-1}{n^2+2} = \frac{4\pi}{3}(\chi_m + N_t\alpha_{pg} + \Delta\alpha_p N_{ex}), \tag{2}$$

where the term in parentheses is given by Eq. (1), considering $N_{ex} = N_t - N_g$ and $\Delta\alpha_p = \alpha_{pex} - \alpha_{pg}$. We can write

the refractive index as $n = n_o + \Delta n$, where the refractive index of the unpumped crystal n_o (when $N_{ex} = 0$) is given by $n_o^2 = 1 + 4\pi f_L(\chi_m + N_t \cdot \alpha_{pg})$ and $f_L = (n_o^2 + 2)/3$ is the Lorenz local field correction factor. The refractive index change Δn is proportional to the susceptibility change due to the excited state population, $\Delta\chi = \Delta\alpha_p.N_{ex}$, and is given by [10]

$$\Delta n = \frac{2\pi}{n_0} N_{ex} f_L^2 \Delta\alpha_p. \tag{3}$$

If we consider an unsaturated pump regime, which is thus $I \ll I_s$ with the pump saturation intensity given by $I_s = h\nu/\sigma\tau$, then $N_{ex} \sim N_t I/I_s$. Therefore, Δn is proportional to the intensity and can be written similarly to the Kerr nonlinear effect, $n = n_o + n_2 I$, with [15]

$$n_2 = \frac{N_t}{I_s}\left(\frac{2\pi}{n_o} f_L^2 \Delta\alpha_p - i\frac{\lambda}{4\pi}\Delta\sigma\right). \tag{4}$$

Eq. (4) was written by considering $n_2 = n_2' - in_2''$ as a complex quantity whose imaginary part takes into account the effect of ESA. The absorption coefficient can be expressed as $\alpha = N_g \cdot \sigma_{gsa} + N_{ex} \cdot \sigma_{esa} \sim N_t \cdot \sigma_{gsa} + N_{ex} \cdot \Delta\sigma$, where $\Delta\sigma = \sigma_{\mathrm{esa}} - \sigma_{\mathrm{gsa}}$ is the difference between the ESA and GSA cross sections.

The CTB model first proposed by Pohl to explain the frequency behavior of ruby lasers [6] assumes the single oscillator approximation, which neglects the contribution of all other states but the CTB, so the ground state polarizability is

$$\alpha_{pg}(\bar{\nu}) = \frac{e^2}{m}\sum_j f_{jg} \cdot \frac{1}{\bar{\nu}_{jg}^2 - \bar{\nu}^2} \approx \frac{e^2}{m} f_g \cdot \frac{1}{\bar{\nu}_{CT}^2 - \bar{\nu}^2}, \tag{5}$$

where f_g represents the oscillator strength of the transition between the ground state and the CTB. Similarly, we consider that the excited state polarizability is proportional to f_{ex}:

$$\alpha_{pex}(\bar{\nu}) \approx \frac{e^2}{m} f_{ex} \cdot \frac{1}{(\bar{\nu}_{CT} - \bar{\nu}_{ex})^2 - \bar{\nu}^2},$$

so that the polarizability difference can be written as

$$\Delta\alpha_p(\bar{\nu}) = \frac{e^2}{m}\left[\frac{f_{ex}}{(\bar{\nu}_{CT} - \bar{\nu}_{ex})^2 - \bar{\nu}^2} - \frac{f_g}{\bar{\nu}_{CT}^2 - \bar{\nu}^2}\right], \tag{6}$$

where $\bar{\nu} = 1/\lambda$, and $\bar{\nu}_{ex}$ and $\bar{\nu}_{\mathrm{CT}}$ represent the excited state and CTB energies (in cm^{-1}), respectively.

All the previous works using the CTB model [6,8,17,18] assumed that $f_{ex} \approx f_g$ in order to estimate $\Delta\alpha_p$ from Eq. (6). Weaver and Payne [17], for instance, used this model to fit their dispersion curves of $\Delta\alpha_p(\bar{\nu})$ for three Cr^{3+}-doped crystals by adjusting $\bar{\nu}_{CT}$ and $f_{ex} \approx f_g = f$. For Cr:GSGG, they obtained $\bar{\nu}_{CT} = 45,700\ \mathrm{cm}^{-1}$ and $f = 0.014$, in reasonable agreement with the values obtained from the ESA spectrum provided by Andrews [19], i.e., $\bar{\nu}_{CT} = 48,000\ \mathrm{cm}^{-1}$ and $f \sim 0.03$.

3. GSA/ESA MEASUREMENTS AND ANALYSIS

A. Experimental Considerations

The first technique, which we already described in detail in [20], is a double lock-in amplifier technique that consists in extracting what is called an ESA difference spectrum, $\ln(I_u/I_p)$. Such a spectrum is obtained through the measurement of the intensity of a weak probe beam chopped at a high frequency (typically 1 kHz) and transmitted by the sample while it is pumped (probe intensity I_p) and unpumped (probe intensity I_u) by a pump beam chopped at a low frequency (typically 10 Hz). In the present experiments, pumping was provided by a CW argon ion laser at 488 nm and the probe light by either a tungsten-halogen broadband lamp source between about 350 and 700 nm ($14,280$–$28,500\ \mathrm{cm}^{-1}$) or a deuterium broadband lamp source between about 220 and 450 nm ($22,000$–$45,000\ \mathrm{cm}^{-1}$). With this technique, the ESA difference spectra were registered in both π (probe light electric field $E \| C$ axis of the ruby crystal) and σ ($E \perp C$) polarizations.

The second technique consists again in recording some ESA difference spectra, but resulting from pulsed pump and probe light sources. Details on this time-resolved pump-probe technique and on the procedure that is used to extract the data can be found in [21] and [22]. Pumping is realized with a standard ($1\ \mathrm{cm}^{-1}$ bandwidth, 5 ns pulse duration) GWU model C355 optical parametric oscillator (OPO) pumped by a 10 Hz repetition rate, 10 ns pulse duration Q-switched Nd-YAG laser frequency-tripled at 355 nm, and the probe is a synchronized pulsed xenon arc lamp with a 5 μs pulse duration. With this second technique, the sample was excited at about 570 nm, and the ESA difference spectrum was registered with unpolarized light (to be able to reach the shortest wavelengths) between about 180 and 350 nm ($28,500$–$55,500\ \mathrm{cm}^{-1}$). Because below about 250 nm we were at the spectral limit of our grating and reflecting mirrors, ESA measurements were rather delicate. This is the reason why they were made point-by-point by allowing more and more light to go through the pinholes located along the pathway of the probe beam, by opening the slits of the spectrometer, and by increasing the voltage on the detector (photomultiplier) for each measurement.

B. Results Obtained with Ruby

1. Ground-State Absorption Data

The sample used in our experiment was in the form of a platelet 1.11 mm thick, with the crystallographic axis c in the plane of the platelet. According to Cronemeyer's data [23], our sample would contain about 1.25×10^{19} Cr^{3+}ions/cm^3, which means around 0.035 wt. % Cr_2O_3. According to the data of Dodd *et al.* [24], our sample would contain 0.05 wt. % Cr_2O_3, and thus 1.6×10^{19} Cr^{3+}ions/cm^3.

We noticed that, indeed, there was great confusion in the literature concerning that matter [1,23–25]. The spectra reported by Maiman *et al.* [25], the ruby laser's father, and then in the Koechner reference book (see [1], Fig. 2.4), are definitely wrong. In these spectra, there is indeed an inversion between polarizations, and the intensity ratio between the blue and green bands is not correct, probably because the crystal sample was not oriented properly. Maybe this has been known a long time, but we could not find mention of it in any of the literature. In Dodd *et al.* [24], there are absorption coefficients and concentration data, but no spectra. If we are confident in these data, for a 0.051 wt. % Cr_2O_3 sample, which means 1.62×10^{19} Cr^{3+}ions/cm^{3+}, we should have σ-polarized bands around 400 and 550 nm with absorption coefficients of about 2.89 and 2.85 cm^{-1}, respectively. According

to Cronemeyer's paper [23], where spectra were reported in log scale, for a 1.86×10^{19} Cr^{3+}ions/cm^{3+} sample, the same σ-polarized bands appear with absorption coefficients of about 4.5 cm^{-1}, which clearly differ from the Dodd data. Polarized spectra can be also found in Sugano *et al.* (see [26], Fig. 5.9, p. 118). In this case, the σ-polarized bands appear again with absorption coefficients of about 4.5 cm^{-1}, but for a dopant concentration of 0.28 wt. % Cr_2O_3, or 8.92×10^{19} Cr^{3+}ions/cm^{3+}, which is again wrong.

We finally decided to use the Dodd data. They seem more reliable, and they are the ones that have been used the most extensively for describing saturation and ESA measurements [27]. For example, a saturation intensity of 1.5 kW/cm^2 at 514.5 nm is often used or found in the literature, but this value is based on either unpolarized data or experiments made on samples cut into 60° ruby rods, by using a lifetime of 3.7 to 3.8 ms instead of 3.4 ms and/or by using the Cronemeyer data to derive the dopant concentration or the absorption cross section. Liao and Bloom [9] also derived this value for light polarized perpendicular to the c axis of the crystal (σ polarization), but by using ground and excited absorption coefficients found at low temperatures [27], which is not correct. According to the definition of this intensity, i.e., $I_s = h\nu/\sigma\tau$, where σ stands for the absorption cross section at the pump frequency ν and τ for the lifetime of the emitting level, the corresponding literature averaged GSA cross section $\sigma_{gsa} = \sigma$ is found to be equal to about 7×10^{-20} cm^2. According to our polarized absorption data for a dopant concentration of 1.6×10^{19} Cr^{3+}ions/cm^{3+}, 8.75×10^{-20} cm^2 is found instead for σ polarization ($E \perp c$), and 4×10^{-20} cm^2 for π ($E \| c$). With a lifetime of 3.4 ms, we then find the saturation intensities $I_s^{E\perp c} = 1.3$ kW/cm^2 and $I_s^{E\| c} = 2.8$ kW/cm^2. So, in our opinion, the reason why the previous authors used or found an effective saturation intensity of about 1.5 kW/cm^2 very likely comes from the fact that they were working with light nearly but not completely polarized perpendicular to the c axis of the crystal. This is indeed what happens for the instance when one uses samples cut into 60° laser rods.

2. ESA Data and Analysis

The results obtained with the first technique are reported in the Figs. 1 and 2, and those obtained with the second technique are given in Fig. 3.

The absorption difference values $\Delta\alpha$ reported in Figs. 1 and 2 have been obtained by writing

$$\Delta\alpha = \frac{1}{l}\ln\left(\frac{I_u}{I_p}\right) = (\sigma_{gsa} - \sigma_{esa})N_{ex}, \tag{7}$$

where l is the thickness of the sample, σ_{gsa} and σ_{esa} are the ground and excited absorption cross sections at the considered probe wavelength, and N_{ex} is the excited ion density.

In the near-UV spectral region, between about 35,000 and 45,000 cm^{-1} (220–285 nm), the absorption difference values are much larger than in the visible region. Looking at the GSA spectrum of ruby [27], this simply means that the involved ESA cross section in the near-UV is much larger than the ground state one, so that

$$\Delta\alpha \approx -\sigma_{esa}N_{ex}, \tag{8}$$

and the entire spectrum can be transformed and calibrated in units of cross section provided that N_{ex} is known.

This excited state ion density can be estimated either from the experimental conditions (incident and transmitted pump intensities, excited volume) or, as was done in the past by Kushida [28], Huang and Moos [29], and Fairbank *et al.* [27], by working on the R_1 line of ruby by adjusting, for instance, the pump intensity so that the resulting absorption difference for the R_1 laser line is found to be equal to zero. Such an estimation with the double lock-in amplifier technique may be very tricky. We preferred, instead, to calibrate our spectra by starting from those obtained with the second technique and reported in the Fig. 3. In this case, indeed, the incident and transmitted intensities and the excited volume are easily determined by using a standard power meter and beam-profile analyzer. So, by calibrating and analyzing the ESA spectrum reported in Fig. 3, we came to the following conclusions. The near-UV ESA spectrum is clearly made of two overlapping components, and the ESA cross section around 40,400 cm^{-1} is found equal to $(5.3 \pm 1) \times 10^{-18}$ cm^2. This two-band structure is not clearly seen in the spectra reported in the Figs. 1 and 2 and was found neither by Kushida [28] nor by Huang and Moos [29]. This is probably due to limitations in the signal-to-noise ratio and the spectral resolution used to register the spectra in this critical wavelength domain

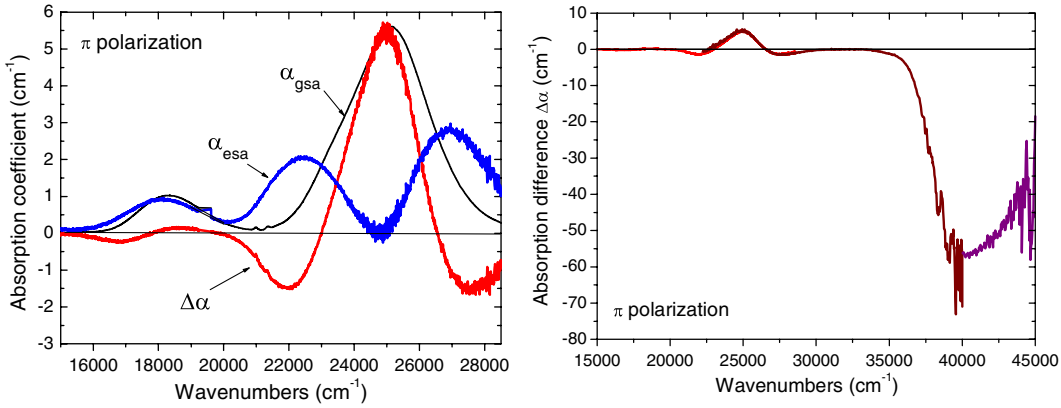

Fig. 1. (Color online) π-polarized GSA (α_{gsa}), ESA (α_{esa}), and absorption difference ($\Delta\alpha = \alpha_{gsa} - \alpha_{esa}$) spectra of 0.05 wt. % Cr_2O_3-doped ruby in the visible and near-UV spectral regions (as obtained with the double lock-in amplifier technique); all the absorption coefficients have been adjusted for a ground or excited state Cr^{3+} ion density of 1.6×10^{19} cm^{-3}.

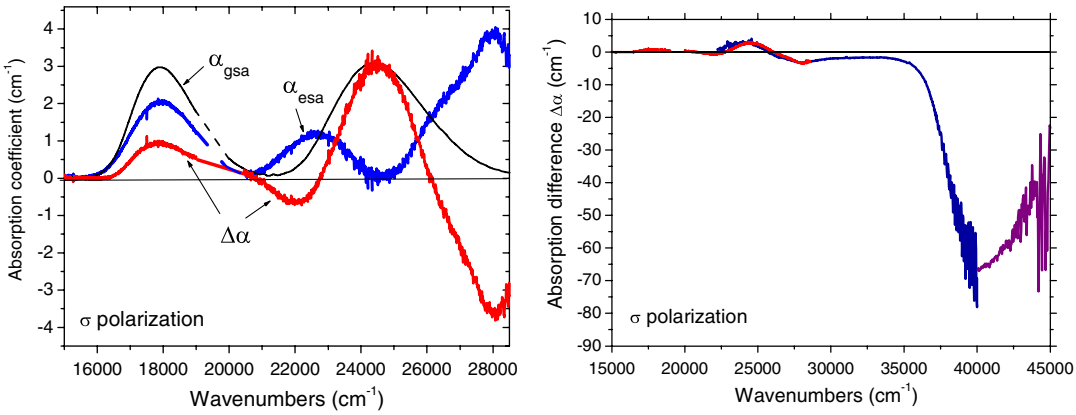

Fig. 2. (Color online) σ-polarized GSA (α_{gsa}), excited-state absorption (α_{esa}) and absorption difference ($\Delta\alpha = \alpha_{gsa} - \alpha_{esa}$) spectra of 0.05 wt. % Cr_2O_3-doped ruby in the visible and near-UV spectral regions (as obtained with the double lock-in amplifier technique); all the absorption coefficients have been adjusted for a ground or excited state Cr^{3+} ion density of 1.6×10^{19} cm^{-3}.

[vacuum UV (VUV) limit]. The spectrum could be fitted with two Gaussian curves peaking around 40,350 and 46, 610 cm^{-1} (248 and 214.5 nm, respectively) and with full widths at half maximum (FWHMs) of about 5467 and 5517 cm^{-1}, respectively. Assuming, then, that the above determined unpolarized cross section (as obtained with the second technique) is the weighted (1/3 and 2/3) average value of the ESA cross sections in the π and σ polarizations, and assuming, according to the results found with the first technique, that the ratio of these cross sections is given by $\sigma_{esa}^{E\perp C}/\sigma_{esa}^{E\parallel C} \approx 1.16$, we ended with the following cross-section values: $\sigma_{esa}^{E\perp C}(250\text{ nm}) \approx 5.6.10^{-18}$ cm^2 and $\sigma_{esa}^{E\parallel C}(250\text{ nm}) \approx 4.8.10^{-18}$ cm^2. These values agree well, in fact, with the calibration made in Figs. 1 and 2, so both techniques reinforce each other. These cross sections, however, are substantially smaller (by about 45%) than that derived in the past by Kushida [28], but very close to that found by Huang and Moos [29].

According to the VUV excitation spectra reported by Loh [30] and Tippins [31], it seems that these two components correspond well to ESA transitions to two charge transfer states located around 7 and 7.9 eV, and thus 56,455 and 63, 714 cm^{-1}, respectively. Indeed, assuming that the excited absorbing state in our experiments is the ^{2}E metastable level of the Cr^{3+} ions, which is located around 14, 400 cm^{-1} (694 nm), ESA transitions to the two considered charge transfer states should occur around 42,055 and 49, 313 cm^{-1}, and thus 238 and 203 nm, in very good agreement, accounting for the Stokes shift likely experienced by each transition, with the energetic positions and separation of the observed ESA bands.

Having calibrated these near-UV ESA bands for both polarizations, and knowing the cross sections σ_{gsa} of the GSA bands for ruby, it is now possible to extract the ESA cross-section spectra σ_{esa} from the ESA difference spectra reported in Figs. 1 and 2 by using Eq. (1). The GSA as well as the resulting ESA spectra have been also added in Figs. 1 and 2.

The oscillator strength can be obtained by [32]

$$f_{g(ex)} = 1.13.10^{12}.\frac{n_o}{f_L^2}\int \sigma_{gsa(esa)}(\bar{\nu})\mathrm{d}\bar{\nu}, \qquad (9)$$

where $f_L = \frac{n_o^2+2}{3}$, with $n_o \approx 1.8$, is the usual Lorentz local correction factor for electric-dipole-allowed transitions. Using the ESA absorption data reported above, it is found that the ESA oscillator strength $f_{ex} = 0.04$.

C. Results Obtained with Cr:GSGG

Gadolinium scandium gallium garnet (GSGG) is a crystal where the Cr impurity occupies a site with low crystal field strength. Therefore, in contrast to ruby, garnet can exhibit a broad fluorescence band at room temperature due to the thermal population of the $^4T_2$ state. Because of the low field strength, the energy gap, $\Delta E = E\left(^4T_2\right) - E(^2E)$, in Cr:GSGG is $\Delta E = 110$ cm^{-1}. The sample was a 1.24 mm thick crystal doped with $N_t = 8 \times 10^{19}$ Cr^{3+}ions/cm^3. The concentration was obtained by comparison of the absorption spectrum with the data of [33].

Here again, we used the two experimental ESA techniques (CW and pulsed) mentioned above. With the double lock-in amplifier technique, pumping was again provided by a CW argon ion laser at 488 nm and thus, as shown in the Fig. 4, on the low energy side of the second absorption band (band assigned to a $^4A_2 \rightarrow {}^4T_{1P}$ transition) of Cr:GSGG. On the other hand, with the second technique, the sample was excited in the red at 610 nm on the high energy side of the first absorption band (band assigned to a $^4A_2 \rightarrow {}^4T_{1F}$ transition). As there is only one type of Cr^{3+} site in Cr:GSGG, the results should be the same with any excitation wavelength. We only used both

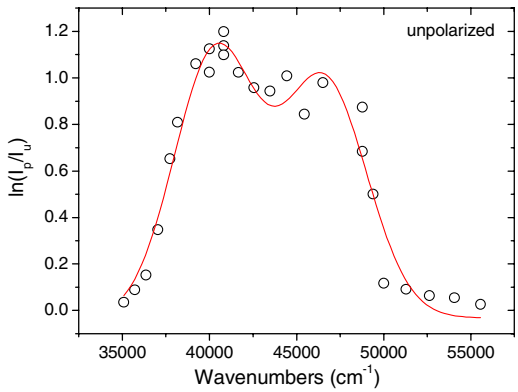

Fig. 3. (Color online) UV ESA difference spectrum of ruby obtained after 570 nm excitation (by using a pump-probe technique with pulsed light sources). Unpolarized probe light.

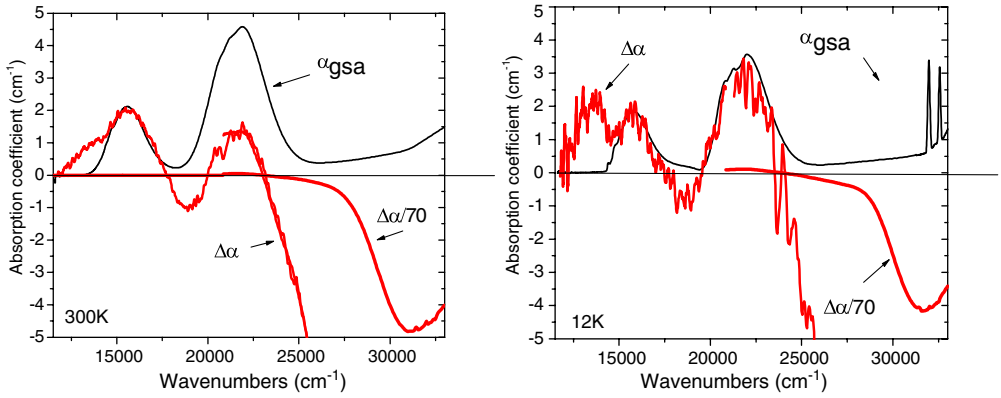

Fig. 4. (Color online) Ground state absorption (α_{gsa}) and absorption difference ($\Delta\alpha$) spectra of Cr^{3+} : GSGG in the visible and near-UV spectral regions (as obtained with the double lock-in amplifier technique) for two temperatures; all the absorption coefficients have been adjusted for a ground or excited state Cr^{3+} ion density of 8×10^{19} cm^{-3}.

techniques to reduce the measurement uncertainties. We show in Fig. 4 only the spectra that have been obtained by using the first (CW) technique, but after calibrating them in absorption coefficient units by using the results obtained with the second one. Moreover, as was already introduced and discussed in Section 1, these spectra have been registered at both low and high temperatures ($T = 12$ and 300 K, respectively). The room temperature spectra are very similar to those obtained in the past by Andrews *et al.* [19]. The present calibration, however, is probably more accurate, since we have been able to register the spectra in a spectral domain, between about 11,750 and 15,000 cm^{-1} (660–850 nm), where our predecessors could not. This spectral domain is very important, indeed, for the calibration of the spectra, since it is where there is neither ESA nor GSA and where gain occurs. By rewriting Eq. (8) as $\Delta\alpha = (\sigma_{gain} - \sigma_{esa})N_{ex}$ with $\sigma_{esa} \approx 0$, we indeed found a peak maximum emission cross section of about 9.5×10^{-21} cm^2 at 760 nm (13,160 cm^{-1}), in perfect agreement with the theoretical estimation and the experimental values that can be found in the literature [19,33,34]. As in [19], the ESA spectra consist of one band in the visible peaking around 19,000 cm^{-1} with an absorption cross section of about 1.25×10^{-20} cm^2 (instead of 3.3×10^{-20} cm^2, as in [19]) and of a very strong one in the near-UV peaking around 32,000 cm^{-1} (312 nm) with a cross section, at $T = 300$ K, of $(4.3 \pm 1.5) \times 10^{-18}$ cm^2 (for 7.8×10^{-18} cm^2 in [19]).

Fitting the near-UV absorption bands obtained at low and high temperatures with Gaussian curves peaking around 315 and 320 nm, and using Eq. (4) with $n/f_L^2 \approx 0.52$, $\sigma_{esa}^{300\ K}(320\ nm) \approx 4.3 \cdot 10^{-18}$ cm^2, and $\sigma_{esa}^{12\ K}(315\ nm) \approx 3.6 \cdot 10^{-18}$ cm^2, it is found that the low and high temperature UV excited state absorption oscillator strengths are $f_{ex}^{12\ K} \approx 1.2 \cdot 10^{-2}$ and $f_{ex}^{300\ K} \approx 1.8 \cdot 10^{-2}$, respectively.

4. Z-SCAN MEASUREMENTS

Z-scan is the most popular technique for measuring the nonlinear refraction index in different kinds of materials [35]. It is a simple and accurate method for the determination of the real and imaginary parts of n_2, based on monitoring the transmission of a laser beam through a nonlinear media. The propagation of a Gaussian beam is affected by the laser-induced refractive index profile, increasing or reducing the on-axis intensity in the far field. The transmittance variation between peak and valley positions is proportional to the induced phase shift through $\Delta T_{pv} \sim 0.406(1 - S)^{0.27}\Delta\Phi_0$, where $\Delta\Phi_0 = kL_{eff}n_2'I_0$, with k as the pump wavenumber, $L_{eff} = [1 - \exp(-\alpha L)/\alpha]$ as the effective length, α as the linear absorption coefficient, n_2' as the real part of n_2, I_0 as the on-axis intensity, and S as the transmittance of the aperture in the absence of a sample. Moreover, the separation between the peak and valley positions is related to the Rayleigh range through $\Delta Z_{pv} \sim 1,7z_0$. When all the light is focused onto the detector, the maximum transmittance variation is related to the imaginary part of n_2 as $T_p - 1 \sim kL_{eff}n_2''I_0$. Therefore, using the shape of the Z-scan curve and the relations above it, is possible to determine the sign and the magnitude of both the real and imaginary parts of the nonlinear refractive index in the material.

For systems with slow response times, such as Cr^{3+}-doped materials [36,37], the time-resolved Z-scan method has proven to improve the sensitivity. The experimental setup is similar to the classical Z-scan one [35], with the introduction of a chopper in order to allow time-resolved detection to eliminate parasitic linear effects [13,38]. As explained before, the refractive index change in Cr^{3+}-doped crystals originates from the metastable excited state, which has a polarizability different from that of the ground state. Therefore, assuming that at $t = 0$ all the population is at the ground state ($N_g = N_t$ and $N_{ex} = 0$), the temporal evolution of the excited state population is given by

$$N_{ex} = N_t(1 - e^{-t/\tau})\frac{I}{I_s}. \tag{10}$$

Eq. (10) is valid in the low pump intensity regime $I \cong I_s$, where the pump saturation intensity is given by $I_s = h\nu/\sigma\tau$. With this method, the transmitted signal is detected at an initial time $t_i \sim 0$ (just after the chopper opening) and at a final time (t_f) in order to obtain the normalized signal $I(t_f)/I(t_i)$ via a data-acquisition system. The parasitic effects are eliminated, because at $t_i \sim 0$ there was not enough time for the long-lived ^2E state to be populated and the transmittance is purely linear; by appropriately choosing $t_f > \tau$ (fluorescence lifetimes), both the linear and nonlinear contributions are present. In this paper, this method was applied to Cr^{3+}:Al_2O_3 (ruby) and Cr^{3+}:GSGG with $\tau = 3.4$ ms and 115 μs, respectively. The Z-scan experiments were performed with either a Kr (647 nm), He–Ne (543 nm), diode (532 nm), or Ar^+ (457, 514, or 528 nm) laser.

A. Z-Scan Results in the Case of Ruby

The Z-scan measurements were performed in two ruby samples with Cr^{3+} concentration $N_t = 1.6 \times 10^{19}$ cm^{-3} (sample 1) and 0.87×10^{19} cm^{-3} (sample 2). Sample 1 was already described in Subsection 3.B.1; sample 2 is a rod with a 5 mm diameter and 3.1 mm length, oriented with the c axis in the direction of the rod.

Figure 5 shows typical data obtained in ruby at 543 nm with a chopper frequency $f = 33$ Hz (the measurements were made at times $t_i = 0.2$ ms and $t_f = 14$ ms after the chopper opening). These data were recorded at a low intensity to avoid saturation effects; the maximum intensity was indeed kept below 90 W/cm^2, which corresponds to ~10% of the I_s value at 543 nm. After its passage through the sample, the beam was split in order to detect both open ($S_1 = 100\%$) and closed (S_2 between 30% and 50%) aperture signals, as is usually done in Z-scan measurements. Following the standard Z-scan procedure [35], the closed aperture signal (S_2) is normalized by dividing it by the (S_1) curve. According to Fig. 5, at 543 nm, it is found that the open aperture (S_1) curve presents a peak in the central position of the Z-scan curve. This indicates that the absorption decreases with intensity. As shown in Fig. 6, the reverse is observed around 457 nm, where the transmittance decreases. In fact, both results obtained at 543 and 457 nm agree with ESA data (Fig. 2). Indeed, according to Fig. 2, for σ-polarized light, i.e., for $E \perp c$ (case of experiments with sample 2), $\Delta\alpha$ (or $\Delta\sigma$) is positive ($\alpha_{esa} < \alpha_{gsa}$) around 543 nm (18,416 cm^{-1}), whereas it is negative around 457 nm (21,881 cm^{-1}).

The values of $\Delta\alpha_p$ and $\Delta\sigma$ were calculated through Eq. (4) by using the n_2 data (real and imaginary parts) obtained from the Z-scan measurements reported in Table 1. It is interesting to note that since $\alpha \approx N_t \cdot \sigma_{gsa}$, then $N_t/I_s \approx \alpha\tau/h\nu$; this means that $\Delta\alpha_p$ and $\Delta\sigma$ can be obtained from the experimental data without the need of N_t, whose calibration may be controversial, as discussed in the previous section.

For ruby we obtained $\Delta\alpha_p \sim 2.0 \times 10^{-25}$ cm^{+3}, and this is found to be approximately constant in the range 543–457 nm. The ~10% fluctuation in the $\Delta\alpha_p$ data presented in Table 1 is lower than the uncertainty of the measurements (~15%).

Measurements were also performed in sample 1 at 514.5 nm in order to investigate the $\Delta\alpha_p$ dependence on the polarization

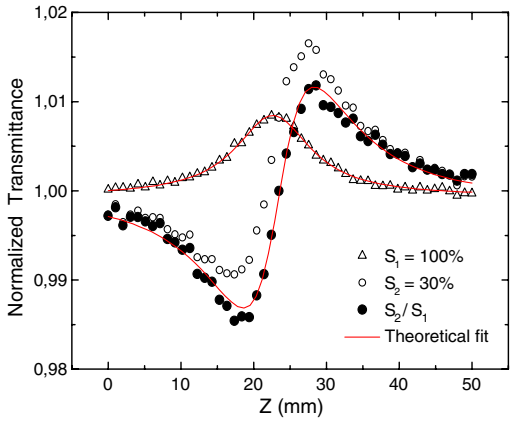

Fig. 5. (Color online) Z-scan results (normalized transmittance) obtained in ruby (sample 2) for laser power $P = 1.55$ mW at 543.5 nm and chopper frequency $f = 33$ Hz. The real part of n_2 is obtained from the theoretical fit of the division curve S_2/S_1 (full circles).

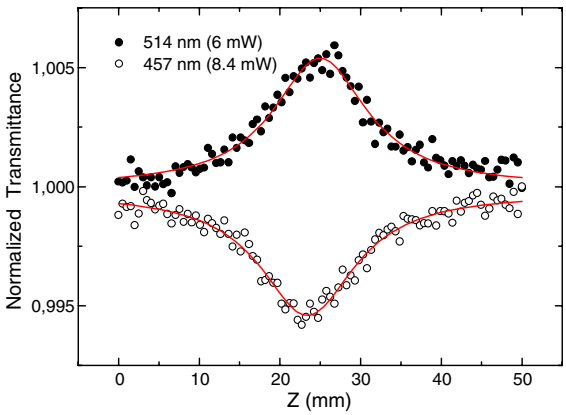

Fig. 6. (Color online) Z-scan measurements with open aperture ($S = 1$) in ruby ($N_t = 0.87 \times 10^{19}$ cm^{-3}). These curves indicate a behavior like saturable absorption for 515 nm, denoting $\sigma_{gsa} > \sigma_{esa}$ and the opposite for 457 nm.

(σ or π). We found that $\Delta\alpha_p$ was about 50% larger for a σ -polarized light. As expected, both samples presented similar $\Delta\alpha_p$ values for the σ orientation.

B. Z-Scan Results in the Case of Cr:GSGG

For Cr:GSGG, we obtained $\Delta\alpha_p = 3.5$, 4.7, and 5.8 (in units of 10^{-25} cm^3) for $\lambda = 647$, 488, and 457 nm, respectively. In this case the spectral dependence of $\Delta\alpha_p(\nu)$ clearly indicates a strong dispersion, similar to that reported in [18]. However, in [17,18], $\Delta\alpha_p \sim 1.1 \times 10^{-25}$ cm^{+3} was reported (for $\lambda =$ 488 nm), which is about four times lower than our value of 4.7×10^{-25} cm^{+3}.

The n_2 value of ruby has been studied extensively by many methods and different research groups [10–16]. There is a good agreement with $\Delta\alpha_p \sim 2.0 \times 10^{-25}$ cm^{+3} at 515 nm, with an ~20% decrease at 633 or 694 nm [7]. In addition, as it is a single-beam technique, the Z-scan data are less sensitive to experimental uncertainties than wave mixing. Therefore, we are confident in the $\Delta\alpha_p$ obtained for both ruby and Cr:GSGG, in this paper.

In Cr^{3+}-doped crystals with low and medium crystal fields, both the $^4T_2$ and ^2E states can be thermally populated, at least at room temperature. This is the case for Cr:GSGG, since the energy difference between the lowest vibrational levels of the $^4T_2$ and ^2E states in this material is $\Delta E = 110$ cm^{-1}, which is comparable with $k_BT \sim 208$ cm^{-1}. Taking the degeneracy of the levels into account, 60% of excited state population is in the $^4T_2$ and the remaining 40% in the ^2E state. However, by cooling the crystal at liquid helium temperature, it is possible to achieve the condition $\Delta E \gg k_BT$ in order to isolate the contribution of the ^2E levels. In ruby, the situation is completely different, since $\Delta E = 3600$ cm^{-1}, and thus $\Delta E \gg k_BT$ even at room temperature, so the $^4T_2$ population is always negligible, and only the ^2E levels can be occupied.

The Z-scan measurements made at low temperatures were not performed by moving the crystal and the cryostat. We instead performed transient measurements with the sample at a fixed position—in fact, at the peak of the Z-scan curve to have a maximum signal (Fig. 7). The transient signal should be proportional to the refractive index change $\Delta n(t)$, which is determined by $N_{ex}(t)$, which is given by Eq. (10). This transient curve is well fit by an exponential with a response time of 118 μs, in conformity with the fluorescence lifetime

Table 1. Z-Scan Data Obtained in Ruby Sample 2 and Comparison with ESA-Derived Values (Sample 1) ($E \perp c$)

λ (nm)	α (cm^{-1})	Z_c (cm)	n_2 (10^{-19} cm^2/W)	$\Delta\alpha_p$ (10^{-25} cm^3)	$\Delta\sigma$ (Z-scan) (10^{-20} cm^2)	$\Delta\sigma$ (ESA) (10^{-20} cm^2)
457	0.14	0.78	$2.6 + 0.16i$	1.8	+3.8	+3.9
514	0.68	0.62	$14.0 - 0.5i$	1.8	−2.0	−2.5
528	1.04	1.6	$23.5 - 1.8i$	1.9	−4.3	−3.4
532	1.13	0.55	$22.2 - 2.0i$	1.7	−4.4	−3.8
543	1.39	0.63	$28.3 - 3.7i$	1.7	−6.3	−4.9

(115 μs). This behavior indicates that the thermal effect is negligible compared to the athermal (electronic) one. Strauss came to the same conclusion in his beam-deflection experiment [39]. In the case of ruby, it is well known that thermal effects are negligible [10,13,15,38].

5. ANALYSIS OF THE RESULTS

A. Case of Cr:GSGG

In most of the cases, the CTB is masked by the fundamental absorption edge of the host material, and it is not possible to accurately determine the oscillator strength f_g of the GSA transition to the charge transfer state. This is the case for Cr:GSGG, since the CTB is located at ~47,000 cm^{-1} and the host matrix is not transparent above 40,000 cm^{-1} (below ~250 nm). Therefore, in this case, the $\Delta\alpha_p$ value is estimated within the CTB model by assuming $f_g \approx f_{ex}$. This is a rough approximation, but it makes sense if we consider that the invoked ground and excited state absorption transitions to the charge transfer (CT) states obey the same selection rules. By doing so in the case of Cr:GSGG, and by inserting $\bar{\nu}_{CT} = 47,000$ cm^{-1} and $\bar{\nu}_{ex} = 44,000$ cm^{-1} in the square brackets of Eq. (6), we find that $\alpha_{pex} \sim 2\alpha_{pg}$ at $\lambda = 632.8$ nm ($\bar{\nu} = 15662$ cm^{-1}). Using the experimental value $f_{\mathrm{ex}} = 0.018$, we obtain $\Delta\alpha_p = 0.9 \cdot 10^{-25}$ cm^3 for $\lambda = 632.8$ nm, which is about four times lower than the experimental value (Subsection 4.B). However, the calculated value has the same order of magnitude as the experimental value, and the approximation $f_g \approx f_{\mathrm{ex}}$ was expected to be a rough one.

We also observed that the oscillator strength of the CTB band was reduced by ~30% when the crystal was cooled down to 12 K ($f_{ex}^{12\ \mathrm{K}} \approx 0.67 f_{ex}^{300\ \mathrm{K}}$). As mentioned before, at room temperature, the $^4T_2$ level is thermally populated, so both excited states ($^4T_2$ and ^2E) contribute to ESA. However, at $T = 12$ K, only the ^2E metastable level is significantly populated, and it is possible to write that $f_{ex}^{12\ \mathrm{K}} \approx f_{2_E}$. At $T = 300$ K, however, the excitation is shared, for 40% by the ^2E energy level and 60% by the $^4T_2$, so that it is possible to write that $f_{ex}^{300\ \mathrm{K}} \approx 0.4 f_{2_E} + 0.6 f_{4_{T_2}}$. Using the above derived proportion between $f_{ex}^{12\ \mathrm{K}}$ and $f_{ex}^{300\ \mathrm{K}}$, it is deduced that $f_{2_E} \approx 0.71 f_{4_{T_2}}$. This result does not agree with the assumption made in [17]: the intensity of the absorption transitions to the CT states should not depend significantly on the selection rules, and thus on the $^4T_2$-^2E energy mismatch.

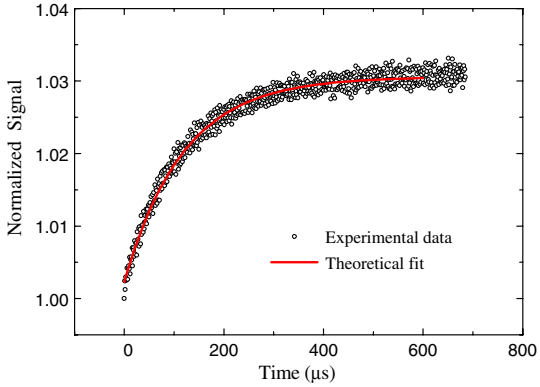

Fig. 7. (Color online) Cr^{3+}:GSGG: transient measurement with the sample fixed at the peak of the Z-scan curve ($T \sim 295$ K, $\lambda_{exc} = 457$ nm, $P_{exc} = 37$ mW). The theoretical fit by Eq. (10) results in $\tau = 118$ μs, in agreement with the lifetime value.

B. Case of Ruby

Again using the approximation $f_g \approx f_{ex} = 0.018$ with $\bar{\nu}_{CT} = 57,000$ cm^{-1} and $\bar{\nu}_{CT} = 14,400$ cm^{-1}, we also obtain $\alpha_{pex} \sim 2\alpha_{pg}$ and $\Delta\alpha_p = 1.5 \times 10^{-25}$ cm^3, which is close to the Z-scan value. However, the case of ruby is more favorable than Cr:GSGG, since the absorption edge of corundum starts above just 7.5 eV and the ligand-to-metal CT band mentioned previously is located around 7 eV. Thus, it is perfectly possible to determine f_g from real absorption data. According to the data reported by Loh [30] and Tippins [31], the cross section of the band peaking around 7 eV ($\bar{\nu}_{CT} = 56,455$ cm^{-1}) and associated with the ESA peak located around 248 nm, would be around 5.5×10^{-17} cm^2, which is huge, and the corresponding oscillator strength would be $f_g \approx 0.3$, and thus nearly 1 order of magnitude larger than f_{ex}. Inserting these oscillation strength values into Eq. (6), the polarizability variation $\Delta\alpha_p$, which should be experienced by ruby when it is pumped into the ^2E metastable level of the Cr^{3+} ions, and thus for $\bar{\nu}_e = 14400$ cm^{-1} (694 nm), and at the He–Ne probe laser wavelength of 632.8 nm ($\bar{\nu}_e = 15662$ cm^{-1}), is found to be negative with the value

$$\Delta\alpha_p = -4.2 \cdot 10^{-25}\ \mathrm{cm}^3,$$

which is rather unexpected, since it is well established that in ruby $\Delta\alpha_p$ is always found to be positive.

6. DISCUSSION

Following the above analysis, the question arises concerning the accuracy of the spectroscopic data and/or of the validity of the CTB model that allows calculation of $\Delta\alpha_p$ [Eq. (6)]. The accuracy of the ESA data is not questionable, at least within some 20% uncertainty. We may doubt the values reported by Loh [30] and Tippins [31], because these measurements were made a long time ago, and they required very delicate experiments performed in the VUV spectral domain with specifically prepared and very lightly doped ruby samples. These results were obtained four years apart and probably with different samples. However, the problem may come from precisely the fact that they are using very different samples compared to ours: samples doped with $N_t = 1.6 \times 10^{18}$ cm^{-3} for Loh, $N_t = 4.7 \times 10^{18}$ cm^{-3} for Tippins, and $N_t = 7.3 \times 10^{18}$ cm^{-3} for Kushida [28], against $N_t = 1.6 \times 10^{19}$ Cr^{3+}/cm^3 in our

case. Cr^{3+} ions in ruby, indeed, are known to form pairs and maybe more complex clusters, already at very low dopant concentrations, and this may impact the probability of the ligand-to-metal charge transfer transitions or the effective ground and excited state ion densities that we use to derive the respective absorption cross sections.

We can also remark that the quantitative determination of f_g is difficult because the absorption is so high that it can be measured only in thin samples with very low Cr^{3+} concentrations, so it might be affected by the presence of unwanted impurities.

Finally, it is necessary to discuss the hypothesis of elastic relaxation proposed by Strauss for Cr:GGSGG [39] and by Eilers *et al.* for Ti:Al_2O_3 [40], using time-resolved beam-deflection spectroscopy. Like the Z-scan, this technique is sensitive to a refractive index modulation and was used to determine Δn due to pumping at 650 nm with a 633 nm probe beam. According to Strauss, the observed effect was electronic (or athermal), since signal transient response agreed with the excited state fluorescence decay time (115 μs). The obtained refractive index change per excited ion per unit volume $\Delta n/N_{ex} = 5 \times 10^{-24}$ cm^3, which according to Eq. (3) corresponds to $\Delta\alpha_p = 4 \times 10^{-25}$ cm^3, is in good agreement with our Z-scan results. However, according to Strauss, Δn is due to the photoelastic effect caused by the elastic dilatation of the CrO_6 cluster in the excited $^4T_2$ state of Cr^{3+}. This explanation is based on a coordinate diagram model, the equilibrium position of the $^4T_2$ being different from that of the ground state ($^4A_2$). In addition, Strauss stated that this effect should not be present in the case of ruby because there is no change of equilibrium position in the ^2E. Our low temperature (ESA and Z-scan) measurements made in the case of Cr:GSGG demonstrated that $\Delta\alpha_p$ is approximately the same for the two different excited states, ^2E and $^4A_2$, which rules out the photoelastic hypothesis as the only source of pump-induced refractive index change.

7. CONCLUSION

We have performed complete ESA and Z-scan measurements in ruby and Cr^{3+} : GSGG in order to investigate the origin of $\Delta\alpha_p$ in these materials. ESA measurements were performed in the visible as well as in the UV spectral ranges to accurately determine the positions (energies) and the oscillator strengths of their CTBs. Measurements in the case of Cr:GSGG were performed at room and low temperatures (12 K) in order to discriminate the contributions of the ^2E and $^4T_2$ states. In addition, Z-scan measurements were conducted at different probe wavelengths across the visible range in the CW as well as in the pulsed regimes.

Our Z-scan results indicate an increase of $\Delta\alpha_p$ with frequency, and stronger values in the case of Cr:GSGG compared to ruby, in good qualitative agreement with the CTB model and previous data reported in the literature. The ESA data obtained in the case of Cr:GSGG at low and room temperatures show that the oscillator strength of the UV excited state absorption transition to the CT state in this material does not vary with temperature by more than 30%. This indicates that it is not significantly affected by the nature (^2E or $^4T_2$) of the starting level of this transition or, thus, by spin selection rules. It means that the $\Delta\alpha_p$ value, as derived from a CTB model in which it is assumed that the oscillator strengths of the ground and excited state transitions to the CT states are nearly equal ($f_{ex} \sim f_g$), does not depend significantly on the $\Delta E = {}^4T_2 - {}^2E$ energy mismatch. This disagrees with the interpretation given in the past in [17]. However, the $\Delta\alpha_p$ value that is derived with the CTB model assuming $f_{ex} \sim f_g$ is quite comparable to that derived from the Z-scan measurements.

The situation is more puzzling in the case of ruby. Indeed, because the absorption edge of the host material is located at sufficiently high energy to allow for a direct measurement of the oscillator strength of the GSA band to the charge transfer state (see [30] and [31]), which is not possible with Cr:GSGG, the CTB model could be applied without any approximation. The result, however, is somewhat surprising, since the oscillator strength of the GSA transition is found to be more than 10 times larger than the ESA one. According to the CTB model, it would result in a negative $\Delta\alpha_p$ value, which is contrary to any previous experimental values. Curiously, a positive $\Delta\alpha_p$ value, very close to the one obtained with Z-scan experiments, could be obtained if the same oscillator strengths were again assumed, as in the case of Cr:GSGG.

The CTB model, based on the calculation of the variation of electronic polarizability experienced by optically pumped Cr^{3+} ions in solids from the ESA data, thus does not systematically provide the expected agreement with the experimental data. Since we cannot rule it out completely, it might have some bands (more in the UV) missing in the calculations, or there might be a contribution coming from a totally different physical mechanism. As a matter of fact, according to some authors [39,40], the refractive index variations observed in optically pumped materials based on transition-metal ions like Cr:GSGG—and also Ti:sapphire (Ti^{3+}:Al_2O_3)—could be attributed instead to a photoelastic effect stemming from the elastic dilation of the CrO_6 cluster in the $^4T_2$ excited state of the Cr^{3+} ions. Indeed, when the ions are brought into this excited state and this dilation occurs, thermal strains are generated and transformed into refractive index changes due to the elasto-optic effect. However, according to that model, a much stronger variation of polarizability should be observed, for instance, in ruby, when the Cr^{3+} ions are pumped into the $^4T_2$ absorption band then directly into the ^2E (R lines). This is contrary to our observations.

In the end, the origin of the purely electronic refractive index changes observed in optically pumped Cr^{3+} (and other transition-metal ion)-doped materials is not yet completely clear and certainly deserves further investigation. In fact, the question also needs to be reconsidered in the case of the Yb^{3+}-doped laser materials that were recently investigated [21,41]. Indeed, the same type of CTB mechanism is invoked to account for the pump-induced refractive index changes observed in these materials, and the same assumption is made about the oscillator strengths to derive the value of the underlying change of polarizability.

REFERENCES

1. W. Koechner, *Solid-State Laser Engineering*, 5th ed. (Springer-Verlag, 1999).
2. H. J. Eichler, P. Gunter, and D. W. Pohl, *Laser-Induced Dynamic Gratings* (Springer-Verlag, 1986).
3. R. C. Powell and S. A. Payne, "Dispersion effects in 4-wave-mixing measurements of ions in solids," Opt. Lett. **15**, 1233–1235 (1990).

4. H. K. Lee and S. S. Lee, "Measurements of the anisotropic nonlinear refractive-index coefficients of ruby," Opt. Lett. **15**, 54–56 (1990).
5. D. J. Bradley, G. Magyar, and M. C. Richardson, "Intensity dependent frequency shift in ruby laser giant pulses," Nature **212** , 63–64 (1966).
6. D. Pohl, "Inversion dependent frequency drifts in giant pulse ruby lasers," Phys. Lett. A **26**, 357–358 (1968).
7. S. M. Lima and T. Catunda, "Discrimination of resonant and nonresonant contributions to the nonlinear refraction spectroscopy of ion-doped solids," Phys. Rev. Lett. **99**, 243902 (2007).
8. T. N. C. Venkatesan and S. L. Mccall, "Optical bistability and differential gain between 85 and 296K in a Fabry-Perot containing ruby," Appl. Phys. Lett. **30**, 282–284 (1977).
9. P. F. Liao and D. M. Bloom, "Continuous-wave backward-wave generation by degenerate 4-wave mixing in ruby," Opt. Lett. **3**, 4–6 (1978).
10. T. Catunda, J. P. Andreeta, and J. C. Castro, "Differential interferometric-technique for the measurement of the nonlinear index of refraction of ruby and $GdAlO_3$:Cr^{3+}," Appl. Opt. **25**, 2391–2395 (1986).
11. I. McMichael, P. Yeh, and P. Beckwith, "Nondegenerate 2-wave mixing in ruby," Opt. Lett. **13**, 500–502 (1988).
12. C. L. Adler and N. M. Lawandy, "Temperature and spectral dependence of the nonlinear index of ruby via nondegenerate 2-wave mixing," Opt. Commun. **81**, 33–37 (1991).
13. L. C. Oliveira, T. Catunda, and S. C. Zilio, "Saturation effects in Z-scan measurements,"Jpn. J. Appl. Phys. **35**, 2649–2652 (1996).
14. S. M. Lima, H. Jiao, L. A. O. Nunes, and T. Catunda, "Nonlinear refraction spectroscopy in resonance with laser lines in solids," Opt. Lett. **27**, 845–847 (2002).
15. V. Pilla, P. R. Impinnisi, and T. Catunda, "Measurement of saturation intensities in ion doped solids by transient nonlinear refraction," Appl. Phys. Lett. **70**, 817–819 (1997).
16. M. Traiche, T. Godin, M. Fromager, R. Moncorge, T. Catunda, E. Cagniot, and K. Ait-Ameur, "Pseudo-nonlinear and athermal lensing effects on transverse properties of Cr^{3+} based solid-state lasers," Opt. Commun. **284**, 1975–1981 (2011).
17. S. C. Weaver and S. A. Payne, "Determination of excited-state polarizabilities of Cr^{3+} doped materials by degenerate 4-wave mixing," Phys. Rev. B **40**, 10727–10740 (1989).
18. R. C. Powell and S. A. Payne, "Dispersion effects in 4-wave-mixing measurements of ions in solids," Opt. Lett. **15**, 1233–1235 (1990).
19. L. J. Andrews, S. M. Hitelman, M. Kokta, and D. Gabbe, "Excited-state absorption of Cr^{3+} in K_2NaScF_6 and $Gd_3Ga_2Ga_3O_{12}$, $Gd_3Ga_2Al_3O_{12}$," J. Chem. Phys. **84**, 5229–5238 (1986).
20. P. Le Boulanger, J. L. Doualan, S. Girard, J. Margerie, and R. Moncorge, "Excited-state absorption spectroscopy of Er3+-doped Y3Al5O12, YVO4, and phosphate glass," Phys. Rev. B **60**, 11380–11390 (1999).
21. R. Moncorge, O. N. Eremeykin, J. L. Doualan, and O. L. Antipov, "Origin of athermal refractive index changes observed in Yb3+ doped YAG and KGW," Opt. Commun. **281**, 2526–2530 (2008).
22. J. Margerie, R. Moncorge, and P. Nagtegaele, "Spectroscopic investigation of variations in the refractive index of a Nd : YAG laser crystal: experiments and crystal-field calculations," Phys. Rev. B **74**, 235108 (2006).
23. Cronemeyer Dc, "Optical absorption characteristics of pink ruby," J. Opt. Soc. Am. **56**, 1703–1705 (1966).
24. D. M. Dodd, D. L. Wood, and R. L. Barns, "Spectrophotometric determination of chromium concentration in ruby," J. Appl. Phys. **35**, 1183–1186 (1964).
25. T. H. Maiman, R. H. Hoskins, I. J. Dhaenens, C. K. Asawa, and V. Evtuhov, "Stimulated optical emission in fluorescent solids. 2. spectroscopy and stimulated emission in ruby," Phys. Rev. **123**, 1151–1157 (1961).
26. S. Sugano, Y. Tanabe, and H. Kamimura, *Multiplets of Transition-Metal Ions in Crystals* (Academic, 1970).
27. W. M. Fairbank, G. K. Klauminzer, and A. L. Schawlow, "Excited-state absorption in ruby, emerald, and Mgo double-bond Cr^{3+}," Phys. Rev. B **11**, 60–76 (1975).
28. T. Kushida, "Absorption and emission properties of optically pumped ruby," IEEE J. Quantum Electron. **2**, 524–531 (1966).
29. J. W. Huang and H. W. Moos, "Absorption spectrum of optically pumped Al_2O_3:Cr^{3+}," Phys. Rev. **173**, 440–444 (1968).
30. E. Loh, "Ultraviolet absorption and excitation spectrum of ruby and sapphire," J. Chem. Phys. **44**, 1940–1945 (1966).
31. H. H. Tippins, "Charge-transfer spectra of transition-metal ions in corundum," Phys. Rev. B **1**, 126–135 (1970).
32. B. Di-Bartolo, *Optical Interactions in Solids* (Wiley, 1968).
33. B. Struve, G. Huber, V. V. Laptev, I. A. Shcherbakov, and E. V. Zharikov, "Tunable room-temperature cw laser action in Cr^{3+}:GdScGa-Garnet," Appl. Phys. B **30**, 117–120 (1983).
34. W. F. Krupke, M. D. Shinn, J. E. Marion, J. A. Caird, and S. E. Stokowski, "Spectroscopic, optical, and thermomechanical properties of neodymium-doped and chromium-doped gadolinium scandium gallium garnet," J. Opt. Soc. Am. B **3**, 102–114 (1986).
35. M. Sheikbahae, A. A. Said, and E. W. Van Stryland, "High-sensitivity, single-beam n2 measurements," Opt. Lett. **14**, 955–957 (1989).
36. C. Jacinto, D. N. Messias, A. A. Andrade, S. M. Lima, M. L. Baesso, and T. Catunda, "Thermal lens and *Z*-scan measurements: thermal and optical properties of laser glasses—a review," J. Non-Cryst. Solids **352**, 3582–3597 (2006).
37. D. N. Messias, T. Catunda, J. D. Myers, and M. J. Myers, "Nonlinear electronic line shape determination in Yb^{3+} doped phosphate glass," Opt. Lett. **32**, 665–667 (2007).
38. L. C. Oliveira and S. C. Zilio, "Single-beam time-resolved Z-Scan measurements of slow absorbers," Appl. Phys. Lett. **65**, 2121–2123 (1994).
39. E. Strauss, "Bulk and local elastic relaxation around optically-excited centers," Phys. Rev. B **42**, 1917–1921 (1990).
40. H. Eilers, E. Strauss, and W. M. Yen, "Photoelastic effect in Ti^{3+}doped sapphire," Phys. Rev. B **45**, 9604–9610 (1992).
41. R. Soulard, R. Moncorge, A. Zinoviev, K. Petermann, O. Antipov, and A. Brignon, "Nonlinear spectroscopic properties of Yb^{3+} doped sesquioxides Lu_2O_3 and Sc_2O_3," Opt. Express **18**, 11173–11180 (2010).